Materials Chemistry and Physics 180 (2016) 173–183

Contents lists available at ScienceDirect

Materials Chemistry and Physics

journal homepage: www.elsevier.com/locate/matchemphys

Tuning the bimetallic amide-imide precursor system to make paramagnetic GaMnN nanopowders

Mariusz Drygas [a], Jerzy F. Janik [a, *], Michal Musial [a], Jacek Gosk [b], Andrzej Twardowski [c, **]

[a] AGH University of Science and Technology, Faculty of Energy and Fuels, Al. Mickiewicza 30, 30-059 Krakow, Poland
[b] Warsaw University of Technology, Faculty of Physics, Koszykowa 75, 00-662 Warszawa, Poland
[c] University of Warsaw, Faculty of Physics, Pasteura 5, 02-093 Warszawa, Poland

HIGHLIGHTS

- New bimetallic precursor system for conversion to GaN/Mn nanopowders was designed.
- Two conversion routes were applied with precursor nitridation at 500, 700 or 900 °C.
- Prepared nanopowders were thoroughly characterized including magnetic measurements.
- The major product was the gallium nitride Mn-doped phase GaMnN with 2–3 at.% of Mn.

ARTICLE INFO

Article history:
Received 24 April 2015
Received in revised form
24 May 2016
Accepted 26 May 2016
Available online 1 June 2016

Keywords:
Nitrides
Nanostructures
Crystal growth
Magnetic properties

ABSTRACT

A bimetallic molecular system made of gallium (III) tris(dimethyl)amide $Ga(NMe_2)_3$ and manganese (II) bis(trimethylsilyl)amide $Mn[N(SiMe_3)_2]_2$ (Me = CH_3, fixed initial Mn-content 10 at.%) was subjected to ammonolysis in refluxing/liquid ammonia. Upon isolation at room temperature, the amide-imide mixed metal precursor was pyrolyzed at elevated temperatures under an ammonia flow by two different routes. Route 1 consisted of a direct nitridation at high temperatures of 500, 700 or 900 °C. In route 2, a low temperature pyrolysis at 150 °C was applied prior to nitridation at the same final temperatures as in route 1. All nanopowders were characterized by XRD diffraction, FT-IR spectroscopy, and SEM/EDX microscopy and analysis. Thorough magnetization measurements in function of magnetic field and temperature were carried out with a SQUID magnetometer. In all samples, the paramagnetic phase of GaMnN was accompanied by an antiferromagnetic by-product linked to a Mn-containing species from decomposition and oxidation of Mn-precursor excess. The Mn-contents in the crystalline GaMnN, *i.e.*, Mn-incorporated in GaN crystal lattice, were of the order of 2–3 at.% mostly independent on the nitridation route whereas the latter had a pronounced effect on amounts of the antiferromagnetic by-product.

1. Introduction

The question of reproducible preparation of diluted magnetic semiconductors including systems based on gallium nitride GaN doped with manganese Mn, abbreviated here for real product mixtures as GaN/Mn and for a specific Mn-doped phase as GaMnN, has been a focus of the remarkable theoretical and experimental effort in the last 15 years or so, and recent reviews of the subject are at hand [1]. Some of the authors of this study contributed in the area by making such GaMnN materials forms as thin films, monocrystals, and microcrystals [2], and some turned their attention to nanopowders [3]. In this regard, the previous studies on GaN/Mn nanopowders were plagued by the formation of the antiferromagnetic MnO by-product due to the application of oxygen bearing manganese precursors [3] or ferromagnetic precipitates such as Mn_xN_y or Ga_xMn_y formed during the growth process [2e]. Based on this experience, recently, a new oxygen-free precursor system was devised and tried by us: the ammonolysis of the mixture of gallium (III) tris(dimethyl)amide $Ga(NMe_2)_3$ and manganese (II) bis(-trimethylsilyl)amide $Mn[N(SiMe_3)_2]_2$ (Me=CH_3) followed by nitriding pyrolysis at elevated temperatures afforded bimetallic nanopowders build on the gallium nitride lattice [4]. Depending on

* Corresponding author.
** Corresponding author.
E-mail addresses: janikj@agh.edu.pl (J.F. Janik), andrzej.twardowski@fuw.edu.pl (A. Twardowski).

http://dx.doi.org/10.1016/j.matchemphys.2016.05.061
0254-0584/

processing conditions, up to a few percent of Mn were found to be incorporated into GaN lattice. However, a retarded transamination with ammonia of the bulky Mn-N($SiMe_3$)$_2$ groups under typical conditions resulted also in some contaminants formed from competing thermal decomposition of such groups. Among them, the amorphous Mn-N-Si-C species were found to be extremely reactive upon exposure to air and, eventually, yielded manganese silicate as an oxidation by-product accompanying the target GaMnN. Some suitably focused modifications of the synthesis method aimed at reducing amounts of the residual N($SiMe_3$)$_2$ groups were thus advisable.

In this report, described is a study on the GaN/Mn nanopowders prepared by, first, ammonolysis in refluxing/liquid ammonia of the bimetallic precursor system Ga(NMe_2)$_3$/Mn[N($SiMe_3$)$_2$]$_2$ with the fixed initial 10 at.% Mn-content and, second, nitriding pyrolysis of the resulting amide-imide precursor by two different routes. Route 1 consisted of a direct nitridation at selected temperatures in the range 500–900 °C. Route 2 included an initial low temperature pyrolysis at 150 °C under NH_3 prior to the high temperature nitridation. The significance of the treatment at 150 °C, an additional ammonolysis step intended to remedy the incomplete transamination in liquid ammonia, was of interest in appraisal of both the extent of Mn-incorporation and by-product formation. It was decided to use the initial 10 at.% Mn-content which constituted an excess of Mn compared to a reference level of Mn-incorporation in the GaN lattice of the order of a few percent, thus, consciously working in the realm of excessive by-products. It was supposed that the Mn-incorporation into Ga-N bond network would take place mostly at low temperature stages of the reactions with liquid ammonia, very much independently on the Mn excess-related decomposition side reactions and by-product formation occurring at elevated temperatures. Measurements of magnetization with temperature and field strength for the substrate powders were anticipated to help in elucidating various magnetic contributions and their structural basis.

2. Experimental

2.1. Synthesis

The synthesis method used to make GaN/Mn powders was based on the anaerobic preparation of pure nanocrystalline gallium nitride GaN by ammonolysis of gallium (III) tris(dimethyl)amide Ga(NMe_2)$_3$ (Me=CH_3) in refluxing ammonia *via* the formation of gallium imide {Ga(NH)$_{3/2}$}$_n$ and nitriding pyrolysis of the latter at elevated temperatures [5]. To achieve the synthesis of Mn-doped materials while conforming to the basic procedure, a mixture of Ga(NMe_2)$_3$ and Mn[N($SiMe_3$)$_2$]$_2$ [6] with a predefined proportion of Mn/Ga was employed. A detailed description of the procedure is included in our preceding exploratory study [4]. In the present study, a 10 at.% Mn-content bimetallic precursor mixture was used to make two series of the powders *via* different pyrolysis routes (Fig. 1). Route 1 was a one-stage pyrolysis under a NH_3 flow, 0.5 L/min, 4 h at 500, 700 or 900 °C, heating rate 5 °C/min, and afforded gray-beige to brownish powders. Route 2 was a two-stage pyrolysis under a NH_3 flow, 0.5 L/min: first stage at low temperature of 150 °C, 18 h and second stage at an elevated temperature of 500, 700 or 900 °C, 4 h, heating rate 5 °C/min, and yielded similarly colored powders.

2.2. Characterization

All product powders were characterized by the standard powder XRD technique with a X'Pert Pro Panalytical diffractometer (Cu K_α source; $2\Theta = 20–80°$). Average crystallite sizes were evaluated

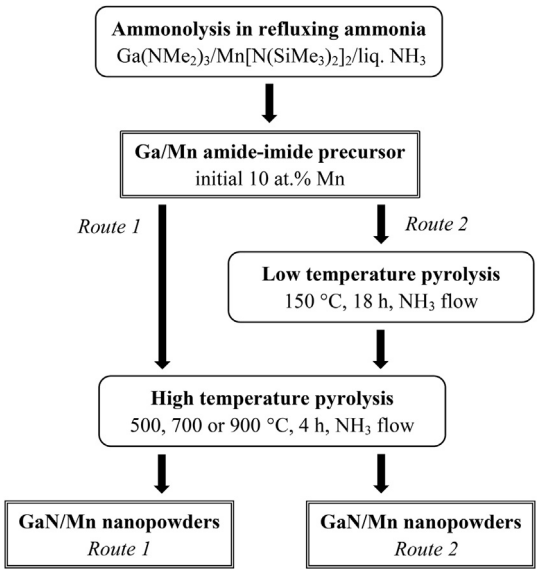

Fig. 1. Scheme of nitridation routes to GaN/Mn nanopowders.

from the Scherrer's equation applying the Rietveld refinement method. For the evaluation, changes of the line profile parameters compared to a standard sample were utilized. Our standard was a polycrystalline alumina sintered body with an average grain size over 5 μm subjected to stress relief annealing. The profile parameters depend on the instrument settings used for data collection and on the profile function used for the refinement. In our analysis the full Voigt function was used to describe the profile of the measured diffraction lines. The total profile width is a convolution of the Gaussian profile part and of the Lorentzian profile part and these parts are combined numerically. In such a method, the full width at half-maximum (fwhm) is only one of several fitted parameters. FT-IR spectra for solids (KBr pellets) were collected on a Nicolet 380 spectrometer. SEM/EDX study was performed using a Hitahi Model S-4700 scanning electron microscope. Magnetization of the samples was measured as a function of magnetic field (up to 7 T) and temperature (2–400 K) using a superconducting quantum interference device magnetometer. The powder samples were placed in gelatin capsules showing controlled diamagnetic signal. To reduce the impact of capsule signal on the measured sample signal, the sample mass was maximized with respect to the upper limit of the SQUID operation range.

3. Results and discussion

The target chemistry behind ammonolysis of the bimetallic system made of gallium (III) tris(dimethyl)amide Ga(NMe_2)$_3$ and manganese (II) bis(trimethylsilyl)amide Mn[N($SiMe_3$)$_2$]$_2$ (Me = CH_3) is based, first, on transamination of the amide groups with ammonia and, second, on multistep condensation of the metal-nitrogen bond network *via* thermally-driven deamination of the NH_2 and NH groups towards the metal nitride lattice. For example, it can be sketched in a simplified way for trivalent Ga (III) that Ga(NMe_2)$_3$ + 3NH_3 → Ga(NH_2)$_3$ (+ ↑3$HNMe_2$) → Ga(NH)$_{3/2}$ (+ ↑3/2NH_3) → GaN (+ ↑1/2NH_3). A very much similar pathway could be individually realized for a divalent Mn (II)-derivative, although, in this case a respective bis(dimethyl)amide derivative is unknown. That was the reason to use, instead, a related and available manganese (II) bis(trimethylsilyl)amide [6]. Our earlier study on the individual ammonolysis of this precursor confirmed the very efficient transamination/deamination processes and the

formation of nanocrystalline manganese nitride η-Mn_3N_2 already after nitriding pyrolysis at 150 °C [7].

Deamination reactions in a mixed metal amide system could, however, be more complex including intermetallic condensation processes. Upon reactions in liquid NH_3, the *in-situ* formed unstable Ga-NH_2 moieties could undergo deamination either of the type Ga-NH_2 + $[(Me_3Si)_2N]$-Mn → Ga-N(H)-Mn (+ ↑H[$N(SiMe_3)_2$]) or according to Ga-NH_2 + H_2N-Mn → Ga-N(H)-Mn (+ ↑NH_3). Such a course is anticipated based on the fast transamination of Ga-NMe_2 to Ga-NH_2 followed by deamination and gallium imide formation at room temperature [5a] whereas for the manganese silylamide derivative the Mn(NH_2)[$N(SiMe_3)_2$](NH) species were isolated under similar conditions [7]. Also, quite feasible could be other transamination reactions such as Ga-NMe_2 + $[(Me_3Si)_2N]$-Mn → Ga-$N(SiMe_3)_2$ + Me_2N-Mn or Ga-NMe_2 + H_2N-Mn → Ga-NH_2 + Me_2N-Mn with the latter mixture possibly deaminating to Ga-N(H)-Mn and ↑$HNMe_2$. In all these cases, there are advantageous conditions for the Ga-N(H)-Mn mixed metal-nitrogen bond formation. In this regard, such chemistry was earlier confirmed by us in the system gallium (III) tris(dimethyl)amide/aluminum (III) tris(dimethyl)amide which upon reactions with ammonia afforded solid solutions of GaAlN at elevated temperatures [5b].

3.1. FT-IR spectroscopy for precursors

The nature of the air-sensitive mixed-metal precursor and its thermal stability at ambient and increased temperatures were conveniently followed by FT-IR spectroscopy. In Fig. 2, the FT-IR spectra for the bimetallic precursor obtained after ammonolysis in refluxing ammonia and stabilization at room temperature (left), and upon its subsequent low temperature pyrolysis under ammonia at 150 °C (right) are shown.

The FT-IR spectrum for the room temperature precursor (Fig. 2, left) shows the strong diagnostic peaks for residual $N(SiMe_3)_2$ groups at *ca.* 2954 cm^{-1} (C-H stretch) and 1250 cm^{-1} (Si-CH_3 deformation) relative both to the N-H stretch peak in the imide =NH groups at *ca.* 3190 cm^{-1} and the Ga-N stretch peak in the evolving gallium-nitrogen lattice at 558 cm^{-1}. This is consistent with an incomplete transamination of silylamide groups in Mn$[N(SiMe_3)_2]_2$ and, at the same time, with a quite efficient deamination of the gallium amide groups Ga-NH_2 and formation of the gallium imide species Ga-N(H)-Ga. As discussed in our initial report about this system [4], there is one new peak in the spectrum at 754 cm^{-1} which is absent in the spectra of both the pure gallium imide and the pure product from ammonolysis of Mn$[N(SiMe_3)_2]_2$ isolated at room temperature. This peak was tentatively assigned to the Mn-N stretches in the bimetallic linkages Ga-N(H)-Mn. Such linkages could be formed by various routes as earlier discussed, for instance, *via* deamination of the type Ga-NH_2 + H_2N-Mn → Ga-N(H)-Mn + ↑NH_3. The additional credentials for this are lent from the absence of easily discernible bands for potential Mn-NH_2 groups at 3332 and 3267 cm^{-1} (N-H stretches) and 1564 cm^{-1} (N-H deformation) that are otherwise clearly seen for the related ammonolysis product of pure Mn$[N(SiMe_3)_2]_2$ [7]. Here, the predominant bands for N-H vibrations are observed in the typical regions for the imide =NH groups at 3193 cm^{-1} (N-H stretch) and 1510 cm^{-1} (N-H deformation). The bimetallic precursor appears to be of the amide ($N(SiMe_3)_2$)-imide (NH) type.

The FT-IR spectrum after pyrolysis of this material at 150 °C, NH_3, is characteristic of decreasing intensities of the bands assigned to the Mn-$N(SiMe_3)_2$ groups relative to the imide =NH and Ga-N vibration bands in the evolving gallium imide lattice (Fig. 2, right). Moreover, a new medium intensity band appeared at 1559 cm^{-1} that is typical for N-H deformations in the Mn-NH_2 amide groups. This is consistent with progressing transamination of the residual Mn-$N(SiMe_3)_2$ groups after such a treatment. It is instructive to note that the formation and persistence of these Mn-NH_2 species in the bimetallic system is rather unusual when compared with the facile transamination and condensation reactions of the monometallic system Mn$[N(SiMe_3)_2]_2$/NH_3 towards manganese nitride η-Mn_3N_2 under comparable conditions [7]. The discrepancy could be explained by the fact that the residual Mn-$N(SiMe_3)_2$ groups in the bimetallic system are dispersed enough to yield scarce Mn-NH_2 groups with hindered chances for deamination *via* Mn-NH_2 + H_2H-Mn → Mn-N(H)-Mn + ↑NH_3. In conclusion, the additional nitriding pyrolysis of the bimetallic precursor at low temperatures up to 150 °C helps in removing the residual $N(SiMe_3)_2$ groups, alas, not all of them and yields another precursor of the amide ($N(SiMe_3)_2$/NH_2)-imide (NH) type. At the same time, this treatment does not appear to contribute significantly to the evolution of the primary bimetallic bond network Ga-N(H)-Mn of which extent is mainly determined during ammonolysis in refluxing/liquid ammonia.

3.2. High temperature nitridation

Two routes were used to accomplish high temperature nitridation of the Ga/Mn amide-imide precursor at the selected temperatures of 500, 700, and 900 °C as described in Experimental. The specifics of the routes are shown in Fig. 1.

The powders obtained from the initial 10 at.% Mn-content precursor constitute an advantageous pool of materials for looking into significance of the 150 °C-pyrolysis in the overall nitridation process under the condition of Mn-excess. Based on the earlier discussion of the FT-IR spectra related to this low temperature treatment, it is apparent that the then progressing transamination of residual Mn-$N(SiMe_3)_2$ groups takes place resulting in lower quantities of the silylamide groups compared with the untreated

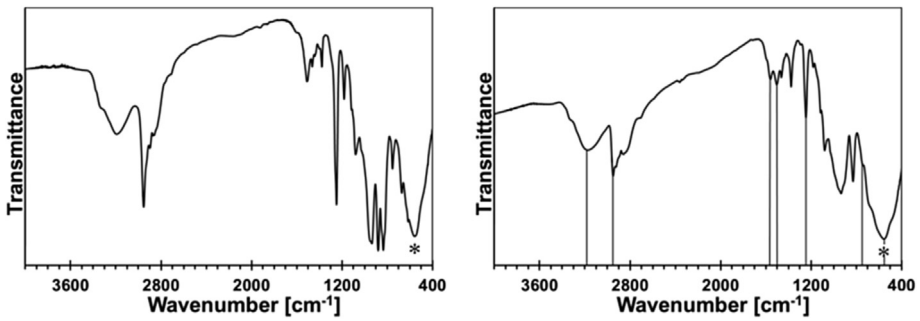

Fig. 2. FT-IR spectra of the bimetallic amide-imide precursor: left – upon isolation at room temperature, right – after pyrolysis under ammonia at 150 °C. Asterisks show the Ga-N stretch, vertical lines in the right are guides to the eye for important bands.

precursor. This should have some influence on the resulting powders prepared at higher temperatures including decomposition by-products formed from different residual groups in each case.

3.2.1. SEM/EDX elemental mapping

Ga, Mn, and Si distributions were investigated with SEM/EDX elemental mapping. The results for the powders prepared at 500, 700, and 900 °C *via* routes 1 and 2 are shown in Figs. 3–5, respectively.

Specifically, Fig. 3 includes results for two related GaN/Mn powders upon pyrolysis at 500 °C. The low magnification images (left, both rows) show typical chunky agglomerates. For the powder made from the room temperature precursor (upper row), the analysis indicates an overall similar distributions of Ga, Mn, and Si. However, there are also agglomerates that are clearly enriched in Mn and, possibly, in Si, which are shown in the ellipsoid. This means that in addition to the prevailing GaN/Mn-bearing phase, GaMnN, the powder contains also some Mn/Si-enriched component. The powder prepared from the °C-pyrolyzed precursor (lower row) appears to have a more homogeneous element distribution.

The EDX elemental mapping for the GaN/Mn powders after pyrolysis at 700 °C is presented in Fig. 4. For the room temperature precursor (Fig. 4, upper row), the Ga and Mn maps appear well matched which supports a high degree of correlation of the element distributions, likely, in GaMnN. At the same time, the Si map shows distinct regions either with relatively enhanced (area in the rectangle) or with very low quantities of Si (voluminous agglomerates in the circle). One may conclude that there is a good correlation between Ga and Mn and, in some areas, between Mn and Si whereas there is no evidence for correlation between Ga and Si so that silicon appears to be likely associated with part of manganese. It is worth mentioning that some carbon C from decomposition of CH_3-containing ligands, under conditions of flowing ammonia, is either to be bound to silicon or to form separate carbon deposits, especially, if suitable temperature conditions for reacting with ammonia are not met.

The elemental mapping for the GaN/Mn powders from the pyrolysis at 900 °C is shown in Fig. 5. Generally, there is a good correlation between the Ga and Mn distributions for the powders from both routes. However, for the room temperature precursor, there are distinct aggregates with Mn and Si, and no Ga (upper row, circles). For the case of the 150 °C-precursor, the resultant powder contains some agglomerates exclusively enriched in Si (lower row, circle and ellipsoid) and amorphous Si-C-containing species can be responsible for it. The pyrolysis at 900 °C provides the powders with the most thermally stabilized phases including both GaMnN, and the Si-C and/or Mn-Si-based by-products.

3.2.2. SEM morphology examination

Representative SEM images for the powders prepared *via* two routes are shown in Fig. 6. Both powders from the 500 °C-pyrolysis are made of large aggregates with a relatively uniform grainy morphology. The grains with sizes from several tens to a few hundred nanometers are agglomerates of nanocrystals that are not resolved in the images. The pyrolysis of the room temperature precursor at 700 °C (route 1) results in usually sharp-ended whisker crystallites a few hundred nanometer long that grow on the surface of large aggregates and form a coral reef-like assemblages. A closer inspection reveals that the interior of the aggregates is made of quite uniform smaller grains. In contrast, a specific feature of the powder made at this temperature from the 150 °C-pyrolyzed precursor (route 2) is its more homogeneous morphology and the lack of surface-related crystal growth seen for the counterpart. The whisker-related growth is found to be enhanced for the powder prepared at 900 °C from the room temperature precursor (route 1). A thick layer of the merged blocky and often hexagonal crystallites with sizes up to several hundred nanometers, often peeled off from interior, is clearly a consequence of similar growth mechanism as seen earlier for the same precursor pyrolyzed at 700 °C. There is a uniform grainy morphology with a much finer size distribution below the surface layer of the large crystals. It is clear that distinct crystal growth mechanisms were operating on the surface and in the interior of agglomerates and resulted in the bimodal morphology features. On the other hand, the powder made at 900 °C from pyrolysis of the 150 °C-pyrolyzed precursor (route 2) does not show the surface-related phenomena and exhibits a quite uniform grainy morphology. Thus, this powder resembles very much its counterpart from pyrolysis at 700 °C. In

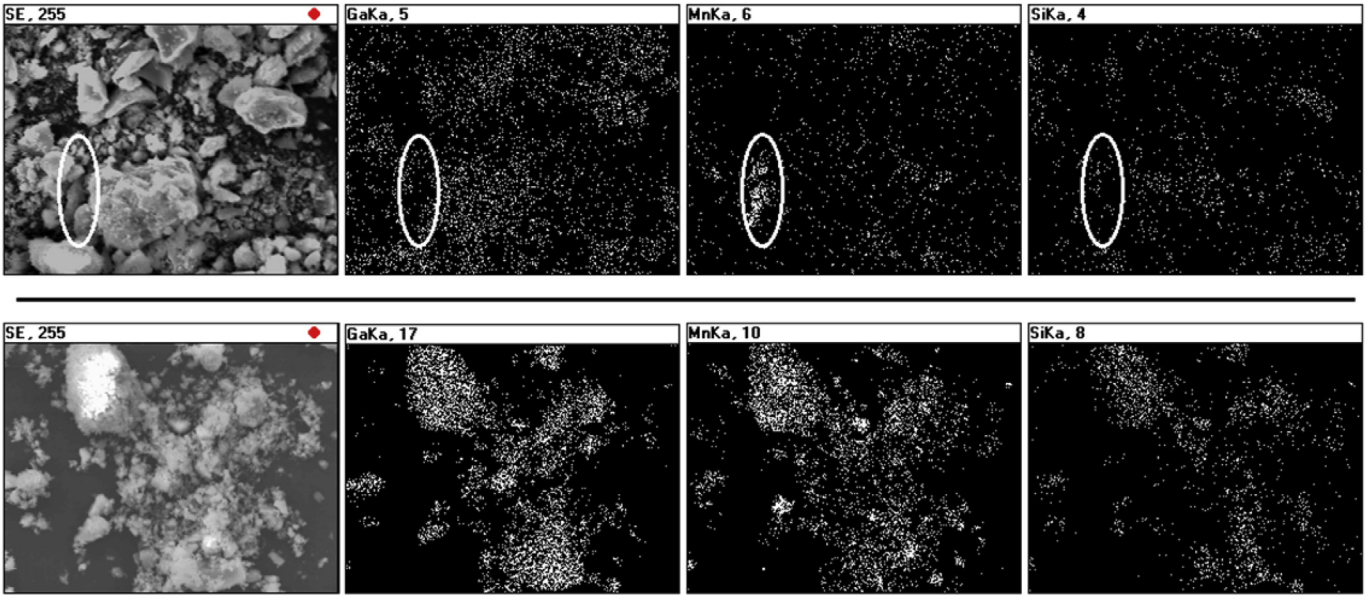

Fig. 3. SEM/EDX elemental mapping for the GaN/Mn powder after pyrolysis of the 10 at.% Mn-precursor at 500 °C, 4 h: upper row – powder from route 1; lower row – powder from route 2. From left to right in each row: SEM image, Ga, Mn, and Si distribution.

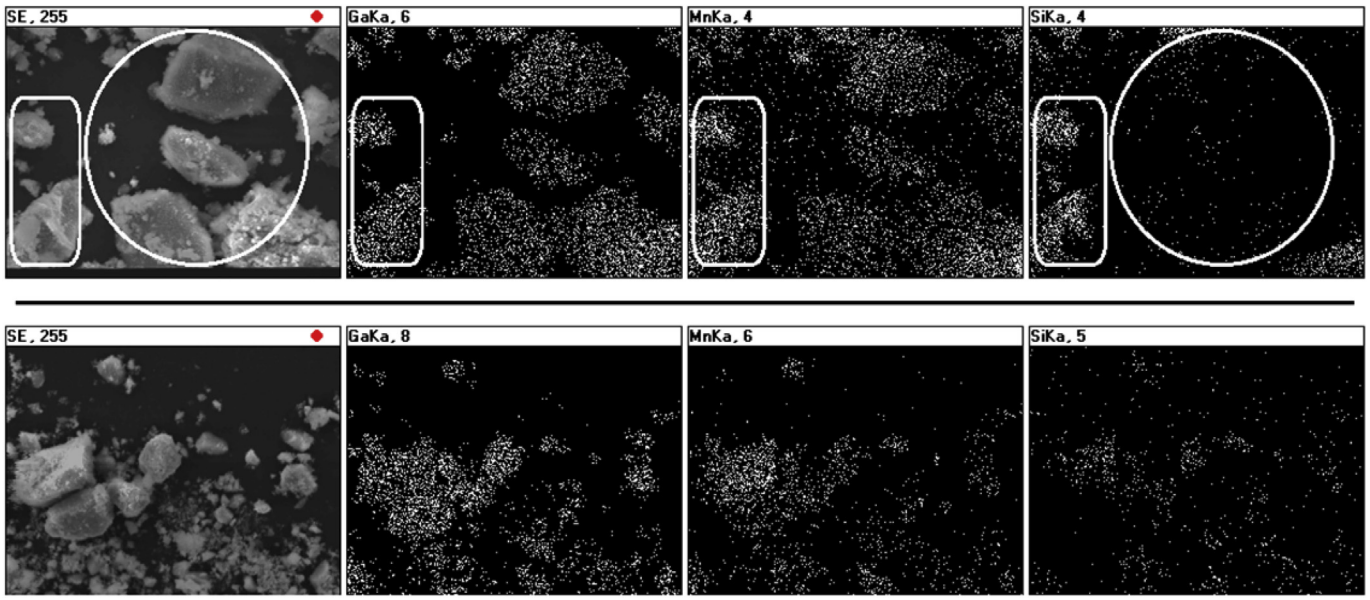

Fig. 4. SEM/EDX elemental mapping for the GaN/Mn powder after pyrolysis of the 10 at.% Mn-precursor at 700 °C, 4 h: upper row – powder from route 1; lower row – powder from route 2. From left to right in each row: SEM image, Ga, Mn, and Si distribution.

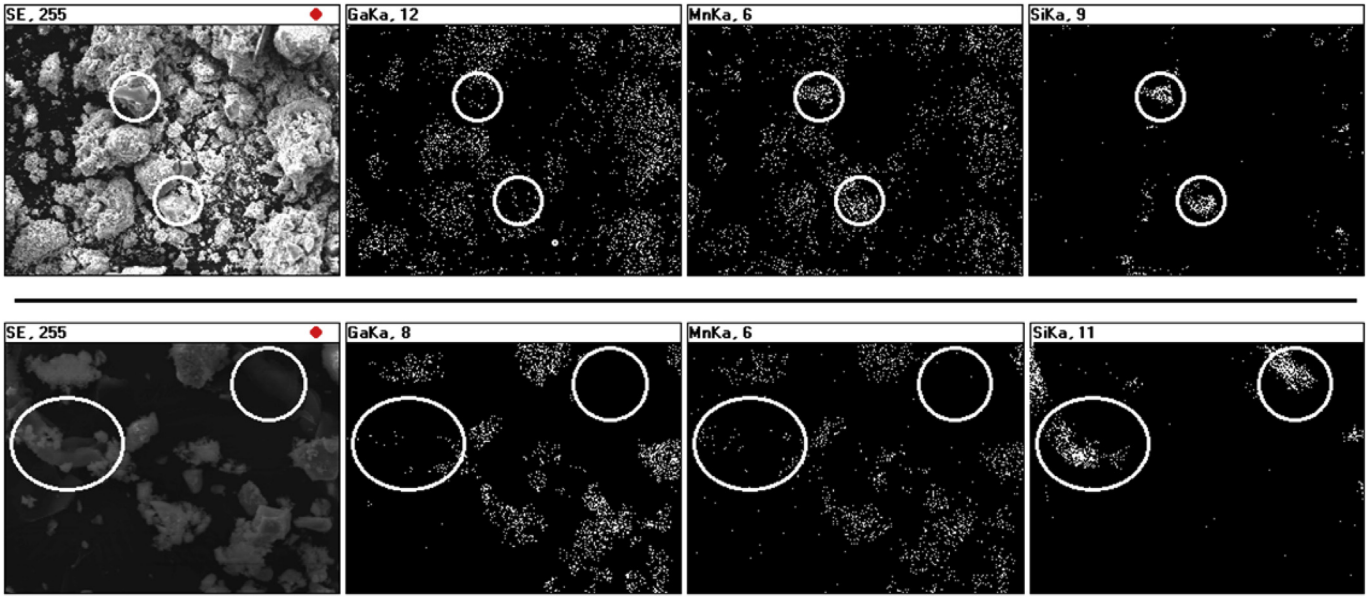

Fig. 5. SEM/EDX elemental mapping for the GaN/Mn powder after pyrolysis of the 10 at.% Mn-precursor at 900 °C, 4 h: upper row – powder from route 1; lower row – powder from route 2. From left to right in each row: SEM image, Ga, Mn, and Si distribution.

conclusion, pyrolysis of the room temperature precursor *via* route 1 yields GaN/Mn powders characteristic of the surface/interior differences in crystal growth whereas the similar treatment of the 150 °C-pyrolyzed precursor *via* route 2 yields powders with a more uniform and homogeneous morphology. It suggests that the chemical nature of the latter retards gas phase reactions/recrystallization of the nitride.

3.2.3. Powder XRD diffraction study

The XRD spectra for the investigated pool of powders are shown in Fig. 7. The essential crystallographic parameters and average crystal sizes for deconvoluted/best fitted phases are included in Table 1.

Some XRD patterns show very broad peaks ("halos") that are typical for nanocrystalline GaN on the verge of crystallinity. They can be described as very small nanocrystallites made of hexagonal and cubic closed-packed layers [5,8] and for the sake of lattice parameter evaluation in this study they are best fitted as cubic c-GaN. In several cases, the deconvolution by best fitting failed to accommodate for real peak intensities and/or actual peak width. This was assumed to result mainly from preferential crystallite growth/texturing that was often confirmed by SEM or by the presence of small quantities of large crystallites. An unusual broadening of peak bases, which was experienced on several occasions, was attributed to bimodal size distribution, *i.e.*, the presence of larger crystallites and much smaller ones that belonged to

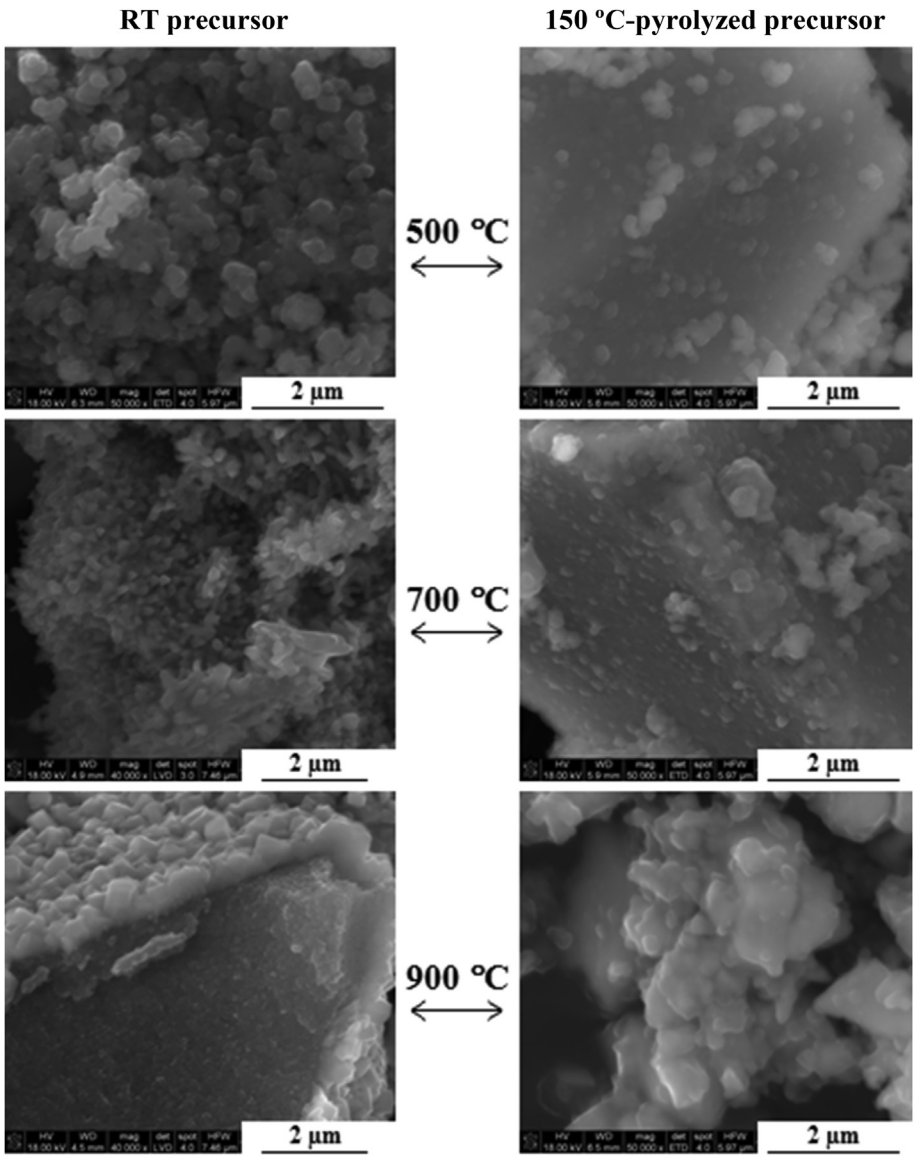

Fig. 6. SEM images of GaN/Mn powders from pyrolysis of 10 at.% Mn-precursor at 500, 700, and 900 °C: left side – route 1, right side – route 2.

two different distribution modes in the nanosize range. Again, such grain characteristics is frequently substantiated by SEM. It is possible that this phenomenon may also result from specific lattice disorders due to small cubic domains incorporated in the predominantly hexagonal GaN-type lattice; however, this kind of structure analysis is beyond the scope of this study. From the outlined perspective, the structure parameters shown in Table 1 should be regarded only as consistent approximations that point out merely to trends without letting strict quantitative assessments.

First, it is evident that all crystalline products detected by XRD are based on the GaN-lattices (phase inhomogeneous, regular, hexagonal); there is not a single case with other detected phases. In this regard, the Mn-Si-enriched particles seen by SEM/EDX in many powders are likely amorphous and/or in small quantities. Also, there are no detectable quantities of any of the manganese nitrides that, theoretically, could be formed from excess manganese in the precursors [7]. Second, the patterns often consist of the unusually broadened and superimposed peaks with base broadening, especially for the 700 and 900 °C pyrolyses, which is consistent with multimodal crystallite size distributions or specific cubic/hexagonal disorders. The data included in Table 1 were calculated by assuming no more than two size distribution modes because more distributions than that, although giving better fits, yielded artificially complex and not otherwise justified results. Based on that, all powders consist of up to two size modes of gallium nitride-based lattices: one with particle diameters of the order of a few nanometers and another one with particle diameters of a few tens of nanometers. It is worth noting that the so-called large nano-GaN in the 900 °C-pyrolyzed powders in Table 1 is characteristic of the average crystallite size of the order of 50–60 nm whereas well faceted crystals of h-GaN with sizes up to several hundred of nanometers are also seen there in the surface layers by SEM. Such large crystals with sharp diffraction lines do not contribute to size-related line broadening and, if present in modest quantities, might have impacted in negative ways the peak intensity deconvolution results. The bimodal size distribution of the GaN-based lattices is undoubtedly linked to the presence of Mn since no such effect has been observed by us for numerous pure GaN powders made by this method.

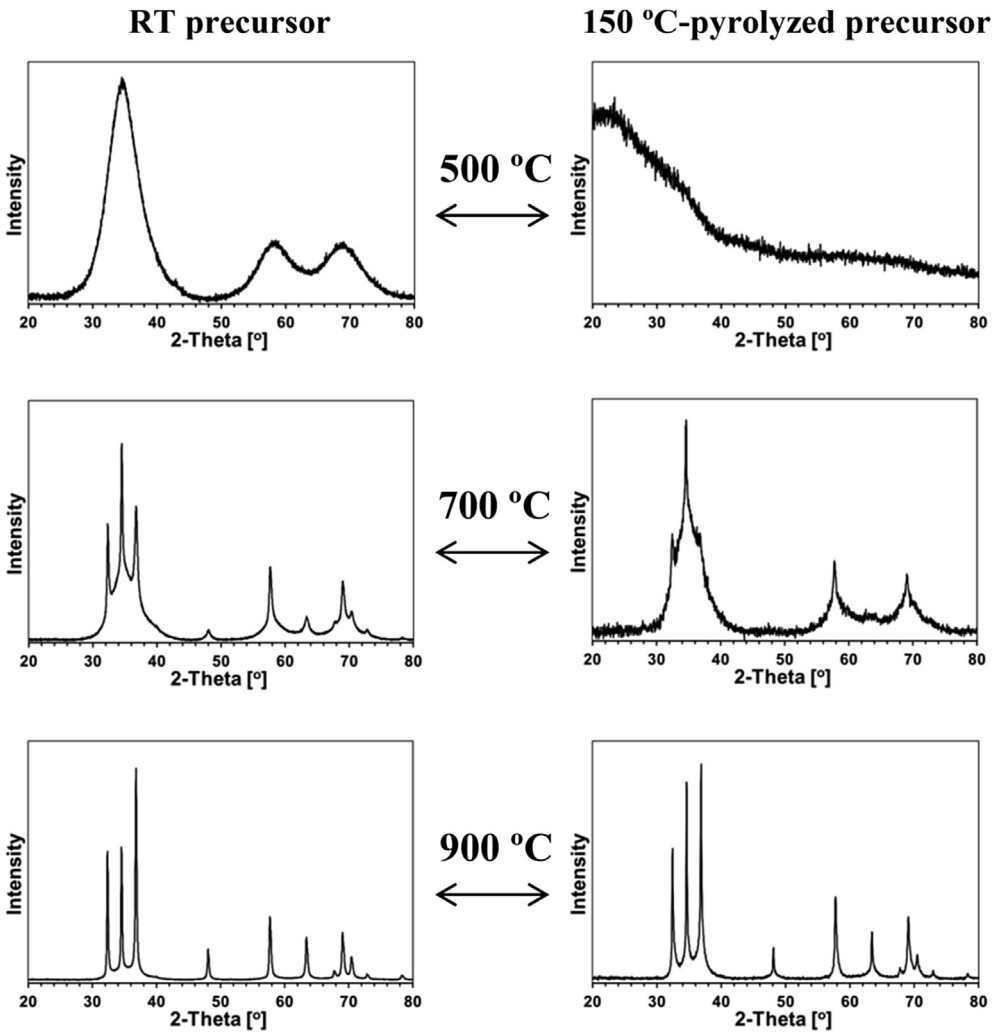

Fig. 7. XRD patterns of GaN/Mn powders from pyrolysis of 10 at.% Mn-precursor at 500, 700, and 900 °C: left side – route 1, right side – route 2.

Table 1
Crystallographic data estimated from XRD patterns of GaN/Mn powders from pyrolysis at 500, 700, and 900 °C *via* routes 1 and 2.

Pyrolysis temperature	GaN/Mn from room temperature precursor (route 1)			GaN/Mn from 150 °C-pyrolyzed precursor (route 2)		
	Phase: Content [%]	Lattice parameters a[Å] c[Å]	Average crystallite size D [nm]	Phase: Content [%]	Lattice parameters a[Å] c[Å]	Average crystallite size D [nm]
500 °C	c/h-GaN (phase inhomogeneous): 100	a = 4.45	1.5	Amorphous powder on the verge of crystallinity	n/d	n/d
700 °C	c-GaN (small nano): 55	a = 4.50	3	c-GaN (large nano): 6	a = 4.54	43
	h-GaN (large nano): 17	a = 3.20 c = 5.19	30	h-GaN (small nano I): 55	a = 3.21 c = 5.22	8
	h-GaN (small nano): 28	a = 3.18 c = 5.18	3	h-GaN (small nano II): 39	a = 3.17 c = 5.92	2
900 °C	c-GaN (small nano): 49	a = 4.46	2	h-GaN (large nano): 37	a = 3.19 c = 5.19	60
	h-GaN (large nano): 51	a = 3.19 c = 5.19	50	h-GaN (small nano): 63	a = 3.19 c = 5.19	5

When comparing the relevant pairs of patterns for a selected pyrolysis temperature (Fig. 7, route 1 *vs.* route 2), it is evident that route 1 yields relatively sharper lines characteristic of better crystallized powders with larger crystallites. It is true starting from 500 °C, where the 150 °C-pyrolyzed precursor resulted in the highly amorphous GaN/Mn with the barely discernible halos, and going to the 700 and 900 °C-derived products with the sharper peaks. This observation is, actually, difficult to explain solely in terms of the thinning effect due to by-products. On the one hand, based on the FT-IR characterization of the room temperature precursor, it contains relatively more residual Mn-N($SiMe_3$)$_2$ groups which upon decomposition might have resulted in larger quantities of amorphous solid by-products inversely impacting crystallization of GaMnN. If true, this would yield powders with smaller average

crystallite sizes and broader diffraction peaks (route 1) than expected for its counterpart (route 2) whereas we observe the opposite. On the other hand, heating under ammonia during initial pyrolysis stages of the room temperature precursor, that is made of a very reactive and not temperature-stabilized network, could have resulted in a more efficient than otherwise removal of volatile by-products before their decomposition has started. Such a course of events would have been somewhat retarded in the 150 °C-pyrolyzed precursor. However, in addition to the thinning argument, the differences in crystallinity/crystallite sizes can also be linked to the target Mn-incorporation into the GaN lattice. In this regards, it is very hard to unequivocally estimate the impact of Mn-centers on GaN lattice parameters since the Mn radius, covalent or atomic, depends also on coordination number and/or high spin/low spin circumstances. Measurements of magnetic properties of the powders could, therefore, shed more light on the problem.

3.2.4. FT-IR spectroscopy for final products

The infrared spectra for the powders prepared *via* both routes are shown in Fig. 8. The opaque characteristics of the KBr pellets is, likely, behind the "waving" of the baseline. The broad and weak peaks at *ca.* 3430 and 1630 cm^{-1} are occasionally seen for adventitious water adsorbed during KBr pellet preparation. The feature at *ca.* 2370 cm^{-1} in the lower left side spectrum is an artifact of background subtraction.

The specific feature of the infrared spectra for the 500 and 700 °C-derived powders is the presence of several bands in addition to the predominant band at 560–590 cm^{-1} for Ga-N stretches in GaN. Perhaps the most diagnostic are the bands at *ca.* 2060–2070 cm^{-1} for Si-H stretches [9] and at *ca.* 940–960 cm^{-1} for Si-N stretches both indicative of side-decomposition species originating from residual Mn-N($SiMe_3$)$_2$ groups. The spectra contain also bands for imide groups =NH, *i.e.*, N-H stretches around 3190–3200 cm^{-1} and N-H deformations around 1500–1520 cm^{-1}. These =NH groups are mostly bound to Si since both Ga and Mn-centers yield, at least individually, the respective metal nitrides or GaMnN at these temperatures.

The 500 °C-powder derived from the room temperature precursor (route 1) appears to contain relatively fewer Si-H functionalities than its counterpart from the 150 °C-pyrolyzed precursor (route 2) as judged from the relative intensities of absorption bands. Interestingly, there are indications that both materials may contain also some amideSi-NH_2 groups based on the presence of the weak peaks at *ca.* 1550–1560 cm^{-1} that are typical for a N-H deformation mode in $-NH_2$.

For the 700 °C-powders, the intensities of the Si-H stretches at

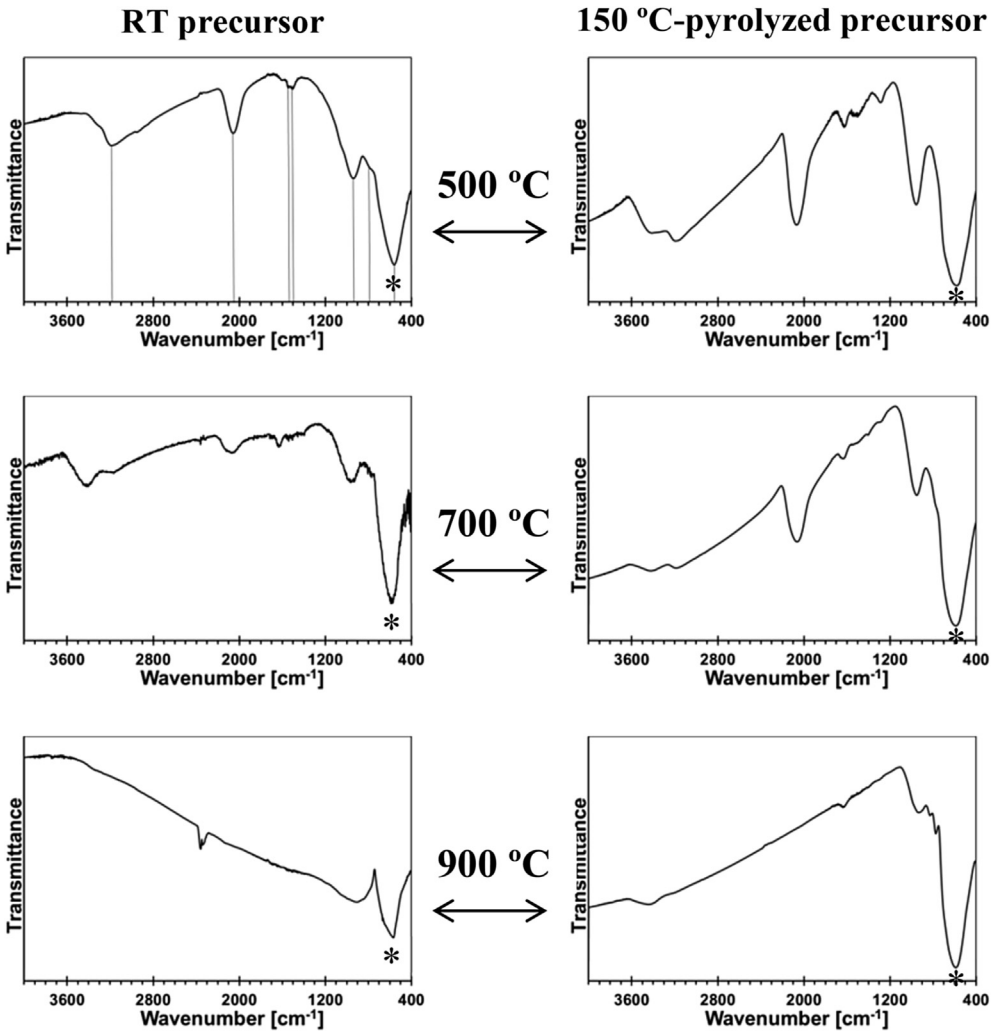

Fig. 8. FT-IR spectra of GaN/Mn powders from pyrolysis of 10 at.% Mn-precursor at 500, 700, and 900 °C: left side – route 1, right side – route 2. Asterisk shows the Ga-N stretch, vertical lines in the upper left are guides to the eye for important bands.

2065 cm^{-1} are lower compared to both 500 °C-powders but, again, the room temperature precursor-derived powder *via* route 1 shows a relatively lower quantity of Si-H than its counterpart made *via* route 2, similarly, as seen earlier for the relevant 500 °C-powders.

The spectra for the 900 °C-powders do not contain bands associated either with Si-H or N-H functionalities which is consistent with their degradation at this temperature to simpler inorganic systems. The predominant band at 575–590 cm^{-1} is linked to Ga-N stretches in GaN lattices. In the spectrum for the route 1-derived powder, there is one more weak to medium intensity broad band at *ca.* 910 cm^{-1} which can be assigned to Si-N stretches in the decomposition by-products. The spectrum for the route 2-derived powder shows three additional bands at 774, 827, and 934 cm^{-1}. The first two bands are in the region of Si-C stretches and the last one is likely to be associated with Si-N stretches. This assignment is consistent with Mn-N-Si-C made-up fragments. In this regard, in our related study on this system we examined also a 50 at.% Mn-precursor and the by-product that was identified with FT-IR and XRD in the 900 °C-pyrolyzed powder was tephroite which is orthorhombic Mn_2SiO_4 [4]. Such a compound could likely form either from the oxidation of the binary nitride $MnSiN_2$ (reported to yield another manganese silicate braunite $Mn^{2+}Mn_6^{3+}SiO_{12}$ [10]) or of the similarly structured amorphous Mn-N-Si-C species.

In conclusion, it is clear that there are differences in the chemical make-up between the composite powders prepared at all pyrolysis levels from the room temperature precursor and from the 150 °C-pyrolyzed precursor. They appear to be mainly associated with initially different quantities of the residual Mn-N$(SiMe_3)_2$ groups and, consequently, with varying final proportions and, to some extent, chemical nature of the amorphous Mn-N-Si-C by-products. The major component in all these cases is a GaN-based product, GaMnN, of which exact nature cannot be deduced from the FT-IR spectra. As stressed earlier in the XRD section, the by-products could, likely, inflict on the crystallization of GaMnN.

3.2.5. Magnetic properties

Magnetization M of the samples was measured as a function of magnetic field B up to 7 T at different temperatures and as a function of temperature (2 K < T < 400 K) for B = 1 T using a SQUID magnetometer. Generally, all measured samples show magnetization composed of both the paramagnetic (PM) and antiferromagnetic (AFM) contributions. There are no indications of disadvantageous ferromagnetic (FM) precipitates/clusters commonly occurring in GaMnN grown by other techniques [2e]. The magnetic features of the nanopowders are similar to those observed earlier in our related study for a wide range of GaN/Mn [4]. As before, we ascribe the PM contribution to Mn-ions incorporated in the GaN lattice whereas the AFM contribution to an antiferromagnetic by-product. It could be inferred from the current magnetization data and the earlier study that the likely by-product is Mn_2SiO_4 – an artifact of excessive quantities of the precursor, its thermal decomposition to reactive species, and oxidation of the latter upon exposure to air. The results of magnetization measurements were qualitatively similar for all currently studied samples. As an example, the data for the nanopowders synthesized at 700 °C *via* both routes are discussed below.

Magnetization in both cases reveals a typical paramagnetic, Brillouin-like behavior. It tends to saturate with increasing magnetic field at the lowest temperatures whereas at higher temperatures (T > 50 K) it is practically linear with magnetic field. However, at T = 2 K it appears to saturate significantly slower than expected for non-interacting Mn-ions in d^5 configuration (Fig. 9, the reference Brillouin function $B_{S=5/2}$ for T = 2 K). The observed slow saturation at the lowest temperatures can be assigned to AFM interactions among Mn-ions in the GaN lattice and/or to some additional linear contribution originating from the antiferromagnetic by-product Mn_2SiO_4. It is of interest to note that in a study on Cr-doping of GaN thin films, the exchange interaction among the implanted chromium centers were of FM character [11].

The AFM interactions are well visualized if magnetization M is plotted as a function of B/T (not shown). For a non-interacting, paramagnetic system all magnetization data should collapse into one curve. This is not the present case as magnetization M *vs.* B/T curves for different temperatures do not overlap. On the other hand, the high temperature data (Fig. 9, T = 200 K and 300 K) reveal an additional linear offset which directly indicates an AFM contribution in the total magnetization.

Another way to demonstrate the AFM-type contribution to total magnetization is to plot M·T as a function of temperature T at constant magnetic field. We recall that for a purely paramagnetic and non-interacting system of magnetic moments, M·T should not depend on T if temperature is not very low. Moreover, the constant value of M·T is related to the number of magnetic centers in the system. On the other hand, interactions in the paramagnetic phase result in M·T bending: downward in the case of AFM interactions and upward for the FM interactions. Such a bending is, therefore, recognized as a signature of interactions among magnetic centers in the PM phase.

In Fig. 10, the M·T *vs.* T experimental data at B = 1 T are shown for samples prepared by both routes (left) accompanied by the same relationships after subtraction of the AFM contribution introduced by Mn_2SiO_4 (right). For each pair of equivalent samples prepared at the same temperature by route 1 and route 2, higher AFM contributions are observed for the samples from route 2 (Fig. 10, left). This stems from the faster increase of M·T with T for the latter, especially, at the highest experimental temperatures. Comparing both route 1 and route 2 samples, the highest total magnetization is revealed by the samples prepared at 700 °C whereas the lowest one by those obtained at 900 °C. On the other hand, Mn-concentrations linked to the PM contribution of GaMnN seem to be slightly higher for the samples prepared *via* route 1. Applying the procedure described in Ref. [4], one can subtract a contribution of the AFM phase from the measured magnetization to get a contribution of the paramagnetic GaMnN phase. The result of such subtraction is shown in Fig. 10, right. The concentration of Mn in the paramagnetic phase can be evaluated for each sample from the high temperature data range (T > 100 K), where the resulting curves are horizontal, neglecting a mass of by-products (not detectable by XRD). However, for both samples prepared at 900 °C a concave shape of the curves (Fig. 10, right) suggests that, in addition to Mn_2SiO_4, another small AFM contribution to total magnetization originating from an unknown AFM phase is conceivable. The estimated proportions of the antiferromagnetic Mn_2SiO_4 and Mn-contents in paramagnetic GaMnN are shown in Table 2.

The Mn-contents in GaMnN are in a rather narrow range of 1.7–3.3 at.% with slightly higher values for the samples obtained by route 1. The present concentration range can be confronted with our earlier study where even for the initial 50 at.% Mn-content a comparable Mn doping level was achieved [4]. This is remarkable since sufficient excess of the manganese precursor was purposely used to support high Mn-incorporation. For both routes, the highest Mn-contents in GaMnN are found in the 700 °C-pyrolyzed powders and the lowest ones in the 900 °C-pyrolyzed powders. Such a trend could be a manifestation of a negative temperature effect on Mn doping at temperatures higher than 700 °C. The overall close Mn-contents are consistent with similar doping chemistry very much independent on the low temperature pyrolysis step. It appears that the major chemical events associated with incorporating manganese occur in the initial stages of ammonolysis

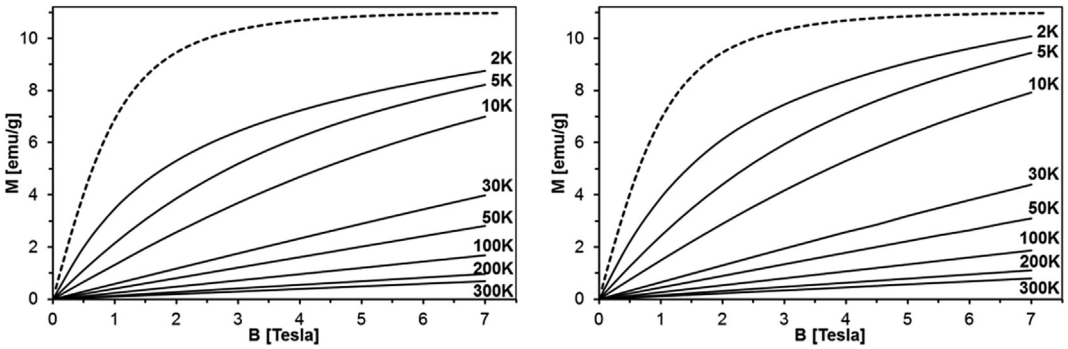

Fig. 9. Magnetization as a function of magnetic field at different temperatures for GaN/Mn powders from pyrolysis of 10 at.% Mn-precursor at 700 °C; left – route 1, right – route 2. The dashed line in both graphs represents a reference Brillouin function with S = 5/2 and reference Mn-content x = 3.3%.

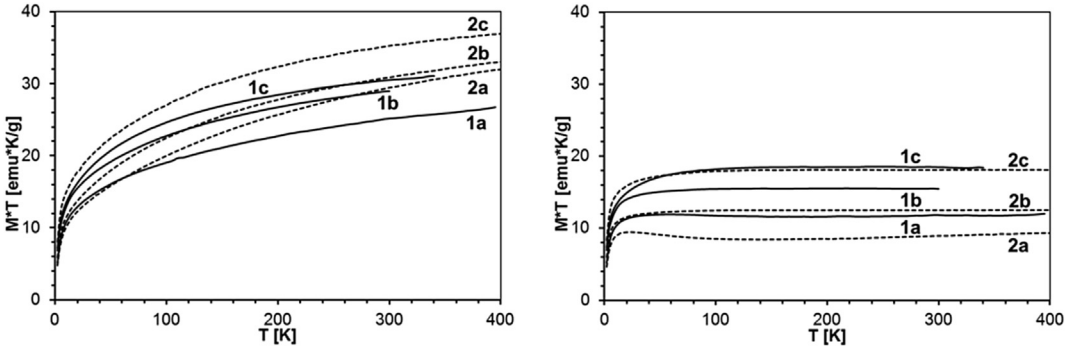

Fig. 10. M·T as function of temperature T at B = 1 T for GaN/Mn nanopowders prepared *via* route 1 and route 2. Left – M·T *vs.* T as measured, *i.e.*, including both PM and AFM contributions. Right – M·T *vs.* T after subtraction of the AFM contribution due to Mn_2SiO_4. 1 – route 1 (—), 2 – route 2 (----); a – 900 °C, b – 500 °C, c – 700 °C.

Table 2
Calculated Mn-contents in paramagnetic GaMnN (at.%) and contents of antiferromagnetic Mn_2SiO_4 by-product (wt%) in nanopowders made *via* route 1 and route 2.

	Route 1			Route 2		
	500 °C	700 °C	900 °C	500 °C	700 °C	900 °C
$wt(Mn_2SiO_4)/wt(sample) \times 100\%$ [wt%]	6.0	5.2	5.7	8.3	8.1	5.7
Mn-content in GaMnN [at.%]	2.7	3.3	2.1	2.2	3.2	1.7

in refluxing/liquid ammonia followed by precursor stabilization at room temperature. The subsequent nitridation pyrolysis *via* route 1 or route 2 impacts after all the conversion of the excess of manganese precursor and the nature of resulting by-products. The latter are composed of some easily oxidized Mn-containing species that upon exposure to air form manganese silicate and of likely N-Si-C-residues of which make-up depends on final nitridation temperature.

Since there were no electric transport studies performed on our powder samples, no conclusions concerning plausible modifications of electrical parameters with Mn doping could be derived. However, having in mind the results of some earlier experiments on GaMnN and GaMnAs, we do not expect the electrical properties such as, for instance, carrier concentration of our samples differ substantially from those for pure GaN.

4. Conclusions

The application of two routes in nitriding conversion of the bimetallic precursor $Ga(NMe_2)_3/Mn[N(SiMe_3)_2]_2$, Me = CH_3, with the fixed initial 10 at.% Mn-content enabled to elucidate major factors behind *in-situ* Mn-incorporation in the condensing Ga-N lattice and, eventually, formation of paramagnetic GaMnN nanopowders. The essential step in the evolution of the Ga-N-Mn bond network is the ammonolysis in refluxing ammonia of the bimetallic mixture. Due to incomplete transamination, some NMe_2 and $N(SiMe_3)_2$ groups are retained in the resultant polymeric amide-imide precursor. The optional low temperature nitridation of the precursor at 150 °C helps in removing additional groups but not all of them and, especially, the $N(SiMe_3)_2$ groups persist in measurable quantities to be decomposed at higher nitridation temperatures to amorphous by-products.

The applied conditions result in GaN-based nanopowders that contain similar quantities of incorporated manganese in the range of *ca.* 2–3 at.% quite independent on reaction details and intermediate nitridation treatment. The optimal nitridation temperature range is 700–900 °C with the upper limit yielding more stable powders but with slightly lower quantities of Mn-contents in GaMnN. There is a noticeable influence of manganese on GaN crystalline phase make-up and this aspect is to be a focus of our further studies.

Acknowledgement

This study was supported by the Polish National Science Centre – NCN, Grant No. 2011/01/B/ST5/06592.

References

[1] a) T. Dietl, H. Ohno, Dilute ferromagnetic semiconductors: physics and spintronic structures, Rev. Mod. Phys. 86 (2014) 187–251 and references therein;
b) T. Jungwirth, J. Wunderlich, V. Novak, K. Olejnik, B.L. Gallagher, R.P. Campion, K.W. Edmonds, A.W. Rushforth, A.J. Ferguson, P. Nemec, Spin-dependent phenomena and device concepts explored in (Ga,Mn)As, Rev. Mod. Phys. 86 (2014) 855–896;
c) A. Hirohata, K. Takanashi, Future perspectives for spintronic devices, J. Phys. D – Appl. Phys. 47 (2014) 193001;
d) S.S. Khludkov, I.A. Prudaev, O.P. Tolbanov, Gallium nitride as a material for spintronics, Russ. Phys. J. 55 (2013) 903–909.

[2] For example, see: a) M. Kaminska, S. Podsiadlo, P. Dominik, K. Wozniak, L. Dobrzycki, R. Jakiela, A. Barcz, M. Psoda, J. Mizera, R. Bacewicz, M. Zajac, A. Twardowski, New chemical method of obtaining thick $Ga_{1-x}Mn_xN$ layers: prospective spintronic material, Chem. Mater. 19 (2007) 3139–3143;
b) S. Podsiadlo, T. Szyszko, W. Gebicki, J. Gosk, R. Bacewicz, L. Dobrzycki, K. Wozniak, M. Zajac, A. Twardowski, Synthesis of bulk $Ga_{1-x}Mn_xN$: a prospective spintronic material, Chem. Mater. 15 (2003) 4533–4535;
c) A. Wolos, M. Palczewska, M. Zając, J. Gosk, M. Kaminska, A. Twardowski, M. Bockowski, I. Grzegory, S. Porowski, Optical and magnetic properties of Mn in bulk GaN, Phys. Rev. B 69 (2004) 115210;
d) M. Zając, J. Gosk, E. Grzanka, S. Stelmakh, M. Palczewska, A. Wysmołek, K. Korona, M. Kamińska, A. Twardowski, Ammonothermal synthesis of GaN doped with transition metal ions (Mn, Fe, Cr), J. Alloy Compd. 456 (2008) 324–338;
e) M. Zajac, J. Gosk, E. Grzanka, M. Kaminska, A. Twardowski, B. Strojek, T. Szyszko, S. Podsiadlo, Possible origin of ferromagnetism in (Ga,Mn)N, J. Appl. Phys. 93 (2003) 4715–4717.

[3] a) J.F. Janik, M. Drygaś, C. Czosnek, M. Kamińska, M. Palczewska, R.T. Paine, Carbothermally-assisted aerosol synthesis of semiconducting materials in the system GaN/Mn, J. Phys. Chem. Solids 65 (2004) 639–645;
b) J.B. Gosk, M. Drygas, J.F. Janik, M. Palczewska, R.T. Paine, A. Twardowski, Magnetic and optical properties of (GaMn)N nanocrystalline powders prepared by the aerosol-assisted vapour phase synthesis and anaerobic imide route methods, J. Phys. D: Appl. Phys. 39 (2006) 3717–3725.

[4] M. Drygas, J.F. Janik, M.M. Bucko, J. Gosk, A. Twardowski, Structural and magnetic properties of GaN/Mn nanopowders prepared by an anaerobic synthesis route, RSC Adv. 5 (2015) 37298–37313.

[5] a) J.F. Janik, R.L. Wells, Gallium imide, $\{Ga(NH)_{3/2}\}_n$, a new polymeric precursor for gallium nitride powders, Chem. Mater. 8 (1996) 2708–2711;
b) J.F. Janik, R.L. Wells, J.L. Coffer, J.V.St John, W.T. Pennington, G.L. Schimek, Nanocrystalline aluminum nitride and aluminum/gallium nitride nanocomposites *via* transamination of $[M(NMe_2)_3]_2$, M = Al, Al/Ga(1/1), Chem. Mater. 10 (1998) 1613–1622;
c) J.L. Coffer, T.W. Zerda, R. Appel, R.L. Wells, J.F. Janik, Micro-Raman investigation of nanocrystalline GaN, AlN, and an AlGaN composite prepared from pyrolysis of metal amide-imide precursors, Chem. Mater. 11 (1999) 20–22.

[6] a) D.C. Bradley, M.B. Hursthouse, K.M.A. Malik, R. Moseler, The crystal structure of bis(hexamethyldisilylamido)manganese, Transit. Met. Chem. 3 (1978) 253–254;
b) H. Chen, M.M. Olmstead, D.C. Pestana, P.P. Power, Reactions of low-coordinate transition-metal amides with secondary phosphanes and arsanes: synthesis, structural, and spectroscopic studies of $[M\{N(SiMe_3)_2\}(\mu\text{-}PMes_2)]_2$ (M = Mn, Fe), $[Mn\{N(SiMe_3)_2\}(\mu\text{-}AsMes_2)]_2$, and $Mes_2AsAsMes_2$, Inorg. Chem. 30 (1991) 1783–1787.

[7] M. Drygaś, M.M. Bućko, M. Musiał, J.F. Janik, Convenient synthesis of nanocrystalline powders of phase-pure manganese nitride η-Mn_3N_2, J. Mater. Sci.-Mater. El. (2016), http://dx.doi.org/10.1007/s10853-016-0094-2.

[8] J.W. Hwang, J.P. Campbell, J. Kozubowski, S.A. Hanson, J.F. Evans, W.L. Gladfelter, Topochemical control in the solid-state conversion of cyclotrigallazane into nanocrystalline gallium nitride, Chem. Mater. 7 (1995) 517–525.

[9] a) Y. Hasegawa, M. Iimura, S. Yajima, Synthesis of continuous silicon carbide fibre, J. Mater. Sci. 15 (1980) 720–728;
b) H.B. Li, L.T. Zhang, L.F. Cheng, Y.G. Wang, Z.J. Yu, M.H. Huang, H.B. Tu, H.P. Xia, Polymer–ceramic conversion of a highly branched liquid polycarbosilane for SiC-based ceramics, J. Mater. Sci. 43 (2008) 2806–2811.

[10] a) R. Pompe, Preparation and TG-DTA analysis of manganese silicon nitride, Thermochim. Acta 16 (1976) 295–300;
b) N.V. Chukanov, Infrared Spectra of Mineral Species: Extended Library, vol. 1, Springer Geochemistry/Mineralogy, 2014, p. 376.

[11] A. Majid, A. Dar, A. Nabi, A. Shakoor, N. Hassan, A. Junjua, J.J. Zhu, Optical, electronic and magnetic properties of Cr:GaN thin films, Mater. Chem. Phys. 136 (2012) 809–815.